IJCFD, 1998, Vol. 10, pp. 45–60
Reprints available directly from the publisher
Photocopying permitted by license only

Large-Amplitude Sloshing in an Oil Tanker with Baffle-Plate/Drilled Holes

T. W. H. SHEU[a] and S.-M. LEE[b]

[a] *Department of Naval Architecture and Ocean Engineering, College of Engineering, National Taiwan University, 73 Chow-Shan, Rd., Taipei, Taiwan, Republic of China;*
[b] *Department of Aerospace Engineering, Tamkang University, Tamsui, Taipei, Taiwan 25137, Republic of China*

(Received 15 October 1996; In final form 28 August 1997)

The sloshing dynamics in a tank partially filled with liquid oil was simulated in this study. The formulation uses primitive variables on a staggered grid system for solving incompressible Navier-Stokes equations, which are subjected to the distortion of free surface. We made use of a volume of fluid technique to resolve numerical difficulties in association with nonlinear free-surface boundary conditions while a two-dimensional quadratic upwind advection scheme to deal with flux nonlinearities. Two problems, namely the free oscillation and the solitary wave propagation, have been chosen for benchmarking the method presented here. The liquid oscillations under conditions of resonance or nonresonance frequency in an oil tanker containing a perforated baffle plate have been studied extensively for two different liquid levels. Through this simulation, we have found that the degree of sloshing can be mitigated by these baffle plates.

Keywords: Incompressible Navier-Stokes equations, free-surface, perforated baffle plate

1. INTRODUCTION

In fluids engineering, there are numerous situations where considerations are warranted concerning the interfaces across which different fluid media exist. Examples include droplet/spray dynamics, metal forming processes, penetration/impact dynamics, rolling with hydrodynamic lubrication, two-phase flows in chemical processes, and of course large-amplitude sloshing analysis. This paper is concerned with the two-dimensional flow of an incompressible fluid in an oil tank for a numerical study of the sloshing phenomena. To allow for surface distortion, we will take the time-varying free surface boundary condition into consideration.

In the sloshing context, oil oscillations in large storage tanks and water oscillations in reservoirs, among other applications, are representative examples of engineering significance. Damage due to such sloshing is reported from time to time. The purpose of conducting sloshing dynamics in an oil tank is twofold. From an economic standpoint, the demand for larger tanks is very great

and calls for a sloshing load analysis for ships classified as LNG carriers, LPG carriers, chemical carriers and the like. From the practical viewpoint, the quest for a free loading under slack conditions is also necessary. Besides numerical difficulties in dealing with nonlinearities in equations for an incompressible viscous flow, the analysis is further complicated by conditions applied at the free surface which is not known a priori. A means capable of analyzing such a nonlinear flow system is, therefore, indispensable for a better understanding the sloshing dynamics in a partially filled oil tank that is subjected to an external force. The mathematical study of free surface began with Lagrange in the early eighteenth century. Since then, substantial progress towards the development of a variable way to track interfaces has been made. Major research efforts have been made, over the past few decades, into the linear study of small amplitude waves and nonlinear theory for shallow water [1]. In the meantime, a new thrust in the application perturbation theory to nonlinear problems raised. As far as the sloshing analyses are concerned, they are mostly based on the potential flow theory [2, 3], which is no longer applicable to oil oscillations under conditions where the viscous effect has a notable impact on the sloshing dynamics. In addition, there is still a considerable obstacle to analytically resolve difficulties regarding nonlinearities In many cases these difficulties are never surmountable. By the 1970s with the wide availability of high-speed computers, there is a hope for coping with problems that were previously intractable. Recent computations have abandoned the simplified working equation in favor of the Navier-Stokes equations.

In the past four decades, there have been substantial developments in predicting free surface flows, among which two major classes of approaches have been frequently referred to. The first approach is that of the Lagrangian formulation in which mass-less particles are traced in illustration the evolution of free surface. The marker and cell (**MAC**) technique of Harlow and Welch [4] is still widely popular among these tracking methods. An attribute of this technique is to distribute the markers in the fluid and to keep track of their subsequent trajectories. Over time, refinements have been made by many authors [5, 6, 7]. The Lagrangian updating process is simple in idea but has the disadvantage of being restricted by a much larger demand for disk storage and CPU time.

The second approach seeks to retain the numerical versatility of the Eulerian description. For methods falling into this category, the high function [8] and the volume of fluid (**VOF**) [9, 10 and 11], approaches are two well-known examples. In the high function approach, it is comparatively easy to conduct derivations. Besides this advantage, extension of the idea of high function to flow problems involving three dimensions is straightforward. This technique is, however, hardly applicable to problems with breaking waves. In the **VOF** approach, the underlying idea is to introduce an additional field variable, whose value stands for the ratio of fluid within a computational cell, so that interface or free surface can be well captured. Of various alternatives, the fractional volume of a fluid is a variable choice. In 1980, a method invoking both Lagrangian and Eulerian computing techniques was proposed to solve problems involving an appreciable change of water surface curvature, but not at the sacrifice of abandoning the merit of the Eulerian technique [12]. Apart from the complexity of implementing this idea into practice, we can not dispense with the numerical diffusion error across the interface in the rezoning step. It seems not yet definite to us if one class of methods should be abandoned in favor of the other free surface tracing methods.

In the present study, we adopted the concept of **VOF** to predict the nonlinear free surface in a partially filled liquid tank. The investigated cases include liquid sloshing induced by a swaying tanker with/without a baffle plate on which several drilled holes may exist. The computed loading owing to the sloshing thus can provide designers with much useful database to conduct stress analysis.

2. GOVERNING EQUATIONS

Working equations capable of rationally describing the dynamics of an incompressible viscous fluid flow are considered. Our concern here is with conservation equations defined in a two-dimensional domain D:

$$\frac{\partial u}{\partial x}+\frac{\partial v}{\partial y}=0, \tag{2.1}$$

$$\frac{\partial u}{\partial t}+\frac{\partial uu}{\partial x}+\frac{\partial uv}{\partial y}=G_x-\frac{1}{\rho}\frac{\partial p}{\partial x}+\nu\left(\frac{\partial^2 u}{\partial x^2}+\frac{\partial^2 u}{\partial y^2}\right), \tag{2.2}$$

$$\frac{\partial v}{\partial t}+\frac{\partial uv}{\partial x}+\frac{\partial vv}{\partial y}=G_y-\frac{1}{\rho}\frac{\partial p}{\partial y}+\nu\left(\frac{\partial^2 v}{\partial x^2}+\frac{\partial^2 v}{\partial y^2}\right). \tag{2.3}$$

In dimensional form, ρ is the density, ν the kinematic viscosity, and p the pressure. In the above two equations, G_x and G_y represent the body forces along the x and y directions, respectively. This mixed set of elliptic-parabolic partial differential equations corresponds to the following generalized equations:

$$\frac{\partial \phi}{\partial t}+\frac{\partial J_x}{\partial x}+\frac{\partial J_y}{\partial y}=S. \tag{2.4}$$

Here, the total fluxes J_x and J_y are defined by $J_x=u\phi-\Gamma(\partial\phi/\partial x)$ and $J_y=v\phi-\Gamma(\partial\phi/\partial y)$. For clarity, the definitions of ϕ and Γ are summarized in Table 2.1.

3. DISCRETIZATION METHOD AND SOLUTION ALGORITHM

For the present analysis based on the finite volume method, the vector quantities (u, v) and scalar variable p are stored in a staggered system [4] to avoid pressure oscillations. The discretized equations for $\phi=(u, v)$ at a point P can be generally represented as follows:

$$\begin{aligned}\phi^{n+1}=&\phi^n+\Delta t(-F\phi X-F\phi Y-DPDN\\&+VISX+VISY)^n+GN.\end{aligned} \tag{3.1}$$

In the numerical approximation of advective fluxes $F\phi X$, $F\phi Y$ by classical central schemes, a spurious pattern of oscillations is resulted for an advection dominated flow. To suppress such oscillations, the upwind formulation should be employed. Enhancement of stability, however, is often accompanied by excessive numerical diffusion errors. Development of an advection model is thus of paramount importance in pursuit of higher simulation quality. To obtain a stable-and-accurate solution for equation (3.1), we have developed a quadratic upwind scheme (**QUICK**$-1/8$) [13] to approximate advective fluxes. The discretization for the nonlinear advective fluxes follows the scheme given below and the reader is referred to Sheu and Lee [13] for additional details:

$$\begin{aligned}F\phi X&=\frac{1}{\Delta x}(u_R\phi_R-u_L\phi_L),\\F\phi Y&=\frac{1}{\Delta y}(u_T\phi_T-u_B\phi_B),\end{aligned} \tag{3.2}$$

where

$$\begin{aligned}u_R&=\frac{1}{2}(u_P+u_E),\ u_L=\frac{1}{2}(u_P+u_W),\\u_T&=\frac{1}{2}(u_P+u_N),\ u_B=\frac{1}{2}(u_P+u_S),\end{aligned} \tag{3.3}$$

$$\begin{aligned}\phi_R=&\phi_{LIN_R}+M_R^+\left[-\frac{1}{8}\phi^+_{CURV_R}+\frac{1}{8}\phi^+_{CURVT_R}\right]\\&+M_R^-\left[-\frac{1}{8}\phi^-_{CURV_R}+\frac{1}{8}\phi^-_{CURVT_R}\right],\end{aligned} \tag{3.4}$$

TABLE 2.1 Definitions

	ϕ	Γ	S
continuity	1	0	0
x-momentum	u	ν	$-(1/\rho)(\partial p/\partial x)+G_x$
y-momentum	v	ν	$-(1/\rho)(\partial p/\partial y)+G_y$

$$\phi_{LIN_R} = \frac{1}{2}(\phi_P + \phi_E), \quad M_R^+ = \frac{1}{2}\left(1 + \frac{u_R}{|u_R|}\right),$$
$$M_R^- = 1 - M_R^+,$$
$$\phi_{CURV_R}^+ = \phi_E - 2\phi_P + \phi_W,$$
$$\phi_{CURV_R}^- = \phi_P - 2\phi_E + \phi_{EE},$$
$$\phi_{CURVT_R}^+ = \phi_N - 2\phi_P + \phi_S,$$
$$\phi_{CURVT_R}^- = \phi_{NE} - 2\phi_E + \phi_{SE}. \tag{3.5}$$

As for the diffusive flux approximation, it suffices to apply a second-order centered scheme to account for their elliptic behavior. In Figure 1, discretization Eqs. (3.4–3.5) render solutions of the same accuracy but a better isotropic phase than does the original QUICK scheme in all wavelengths. We also conduct convergence test for a problem amenable to the analytic solution given by $\phi = 1 - (\ln(x^2 + y^2)/(2 \ln 3))$ in a given velocity field ($u = 2y$, $v = -2x$). According to the computed errors cast in the L_1 and L_2-error norms, the rates of convergence based on the QUICK–1/8 scheme are 2.108 and 2.093, as clearly seen in Figure 2.

To compensate for loss of pressure smoothness owing to the use of standard central differencing for the pressure gradients, one can shift the pressure forward so that pressure solutions are regularized. This is made by adding a curvature term to each pressure gradient term, yielding

$$DPDX = \frac{p_E - p_P}{\Delta x} - \frac{1}{6\Delta x}(p_{EE} - 3p_P + 2p_{\overline{W}}),$$
$$DPDY = \frac{p_N - p_P}{\Delta x} - \frac{1}{6\Delta y}(p_{NN} - 3p_P + 3p_S). \tag{3.6}$$

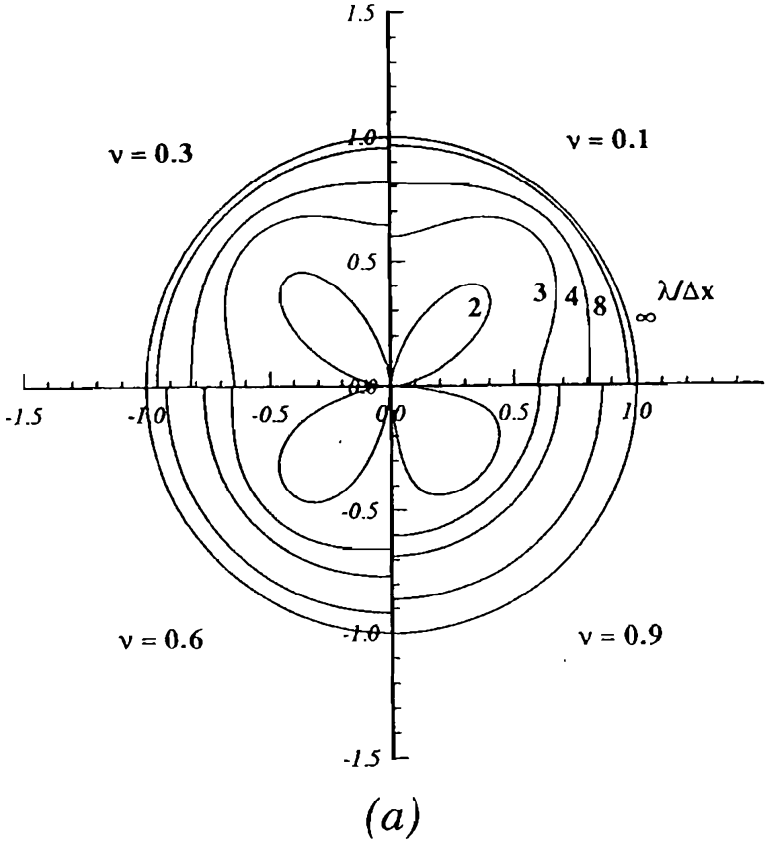

(a)

FIGURE 1 Phase velocity error of the (a) QUICK and (b) QUICK–1/8 schemes for the advection equation in two dimensions.

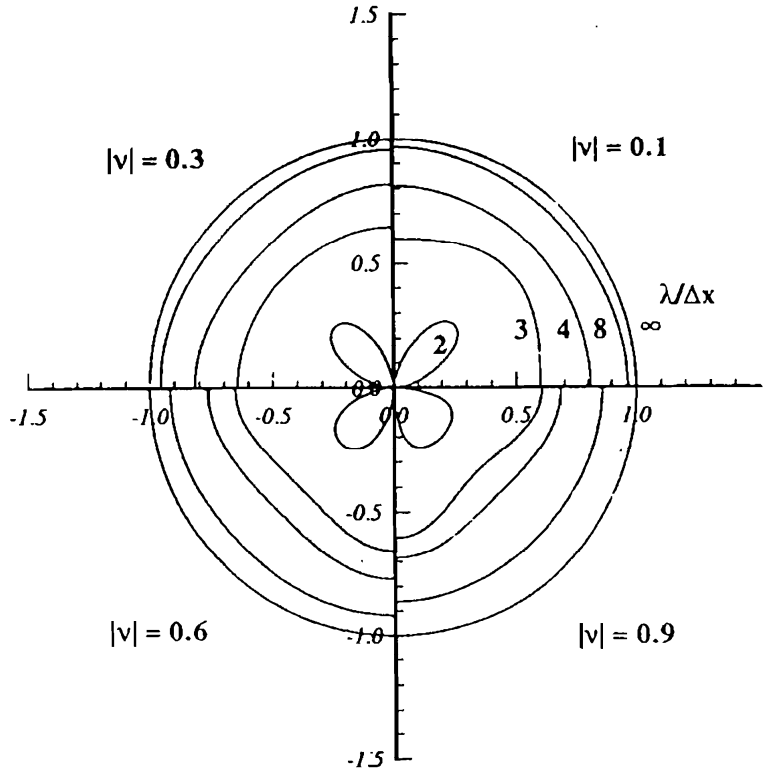

(b)

FIGURE 1 (Continued).

To solve for the primitive variables u, v and p from the coupled Eqs. (2.1–2.3), there are several major solution algorithms for choice. In the present study, we have adopted the segregated approach to solve for the primitive variables in an iterative manner. We first solved for velocities u and v, respectively, from two momentum equations provided an assumed pressure field has been given. With these computed velocities, the discrete zero-divergence constraint condition is not necessarily satisfied. Our strategy to provide a rational amount of pressure correction in Eqs. (2.2) and (2.3) is through the use of continuity equation, yielding a Poisson equation for the pressure correction:

$$\frac{\partial^2 p'}{\partial x^2} + \frac{\partial^2 p'}{\partial y^2} = \frac{\text{Div}}{\Delta t}. \tag{3.7}$$

Worthy to note is that Div $= \partial u^*/\partial x + \partial v^*/\partial y$ is calculated from the most updated velocities.

3.1. Update Procedure for a Cell Full of Liquid Fluid

As is usual, the resulting velocities and pressure are updated according to

$$\begin{aligned} u &= u^* + \frac{\Delta t}{\Delta x}\Delta p', \\ v &= v^* + \frac{\Delta t}{\Delta y}\Delta p', \\ p &= p^* + p'. \end{aligned} \tag{3.8}$$

As the residual Div in Eq. (3.7) approaches asymptotically to zero, the pressure correction is,

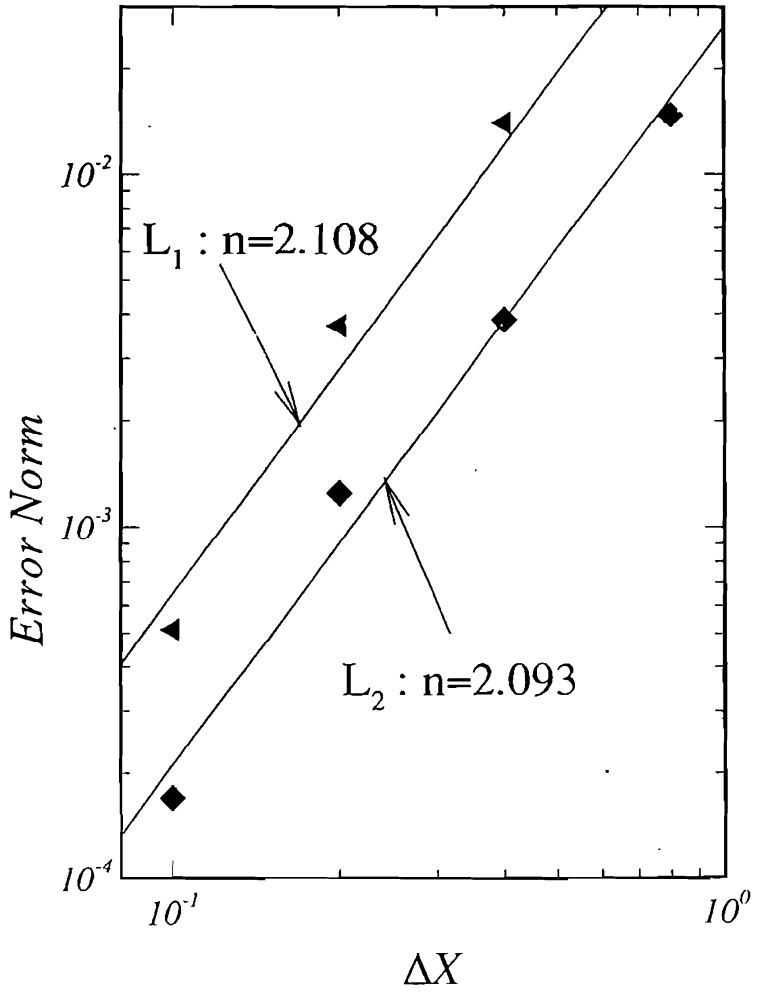

FIGURE 2 Convergence test for the QUICK–1/8 scheme.

thus, no longer needed. This solution algorithm is only applicable to a cell full of liquid fluid.

3.2. Update Procedure for a Cell Containing a Free Surface

Referring to Figure 3, we first define a nondimensional length $\eta = (d_c/d)$, where d_c is the distance between two cell centers while d is the distance from the center of interpolation cell to the nearest free surface of interest. The line connecting the center of the interpolation cell with the center of the free surface cell is closest to the outward normal of the encountered free surface. The pressure in a cell partially filled with water is thus taken as the linear summation of the pressure p_n in the interpolation cell and the pressure p_s at the free surface:

$$p' = (1 - \eta)p_n + \eta p_s - p^*. \tag{3.9}$$

In response to the pressure variation in a free surface cell, velocities vary according to:

$$\frac{du}{dt} = -\frac{1}{\rho}\frac{\partial p}{\partial x}, \qquad \frac{dv}{dt} = -\frac{1}{\rho}\frac{\partial p}{\partial y}. \tag{3.10}$$

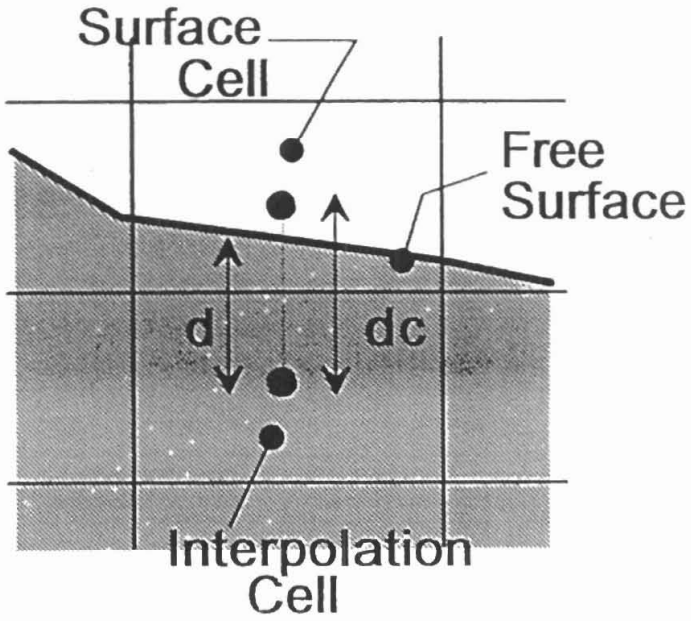

FIGURE 3 Definition used in the free-surface boundary condition.

4. PREDICTION OF FREE SURFACE

To accommodate a deformable free surface below which Navier-Stokes equations hold, we introduce a field variable into the present Eulerian framework to determine the location and the orientation of a free surface. The computed field variable can give us an estimation of the relative absence and presence of the liquid in each computational cell. The chosen fraction volume of the fluid F is defined by

$$F = \frac{V_{\text{liquid}}}{V_{\text{liquid}} + V_{\text{air}}}. \tag{4.1}$$

This field variable follows the following transport equation:

$$\frac{\partial F}{\partial t} + \frac{\partial (uF)}{\partial x} + \frac{\partial (vF)}{\partial y} = 0. \tag{4.2}$$

The entire free surface is depicted by piecewise straight lines which exist in cells containing only the free surface. In each surface cell, the slope of the free surface is computed by

$$\left(\frac{dy}{dx}\right)_i = \frac{\left[(y_{i+1} - y_i)\frac{\Delta x_{i-1/2}}{\Delta x_{i+1/2}} + (y_i - y_{i+1})\frac{\Delta x_{i+1/2}}{\Delta x_{i-1/2}}\right]}{(\Delta x_{i-1/2} + \Delta x_{i+1/2})}, \tag{4.3}$$

where $y_i = y(x_i) = F_{i,j-1}\Delta y_{j-1} + F_{i,j}\Delta y_j + F_{i,j+1}\Delta y_{j+1}$. This enables us to determine the volume of $\eta = d_c/d$. In the present work, we have applied the donor–acceptor concept of Nichols, Hirt and Hotchkiss [11]. On either side of a cell, there exists a donor at the upstream side while an acceptor at the downstream side. Four assignments are invoked to designate the role of acceptor or donor. The objective behind the use of donor–acceptor concept is to preserve a sharp definition of the free surface. Thus, the flux limiter must be prescribed to prevent more gas or liquid than is sufficient from being fluxed out of the donor cell. In order to avoid the negative diffusion error, the cutoff values of F must be prescribed [10 and 11].

5. COMPUTED RESULTS

In fluid engineering, very few problems can be obtained analytically. In this study, we will conduct some of them to benchmark the computer code.

5.1. Free Oscillation

As shown in Figure 4, the filling height of the liquid in a rectangular liquid basin of width 1 is set to be 1. We will consider herein the case with the following-free surface $h(x,0)$ [14]:

$$h(x) = A\sin\left(\frac{\pi x}{4}\right), \tag{5.1}$$

where $A(=0.01)$. The calculation was featured by the time increment $\Delta t = 0.001$ and the spatial spacings $\Delta x = 0.0125$, $\Delta y = 0.005$. As seen in Figure 5, the time-varying heights of the free surface at two vertical ends are referred to as being periodically. For completeness, we also considered the case with the fluid viscosity of 0.01. Clearly revealed from Figure 6 is that free surface heights decrease asymptotically with the increase of time.

5.2. Solitary Wave Propagation

Study of the propagation of a solitary wave in a rectangular channel of uniform depth has received much attention for two reasons [15]. This analysis can provide engineers with useful data about wave loadings to offshore structures. The problem under consideration is configured in Figure 7 where the undisturbed water height d is (1/16) of the channel width. Above the adjacent undisturbed water level, the crest of the solitary wave is given by

$$y = d + H\,\mathrm{sech}^2\left[\sqrt{\frac{3}{4}\frac{H}{d^3}}\,x\right]. \tag{5.2}$$

Here, we consider $H(=2)$ and $d(=10)$ which denote the initial wave height and the still water depth, respectively. Initially, the velocities are given by

$$\begin{aligned} u &= \sqrt{gd}\frac{H}{d}\,\mathrm{sech}^2\left[\sqrt{\frac{3}{4}\frac{H}{d^3}}\,x\right], \\ v &= \sqrt{3gd}\left(\frac{H}{d}\right)^{3/2}\left(\frac{y}{d}\right)\mathrm{sech}^2 \\ &\quad \left[\sqrt{\frac{3}{4}\frac{H}{d^3}}x\right]\tanh\left[\sqrt{\frac{3}{4}\frac{H}{d^3}}\,x\right], \end{aligned} \tag{5.3}$$

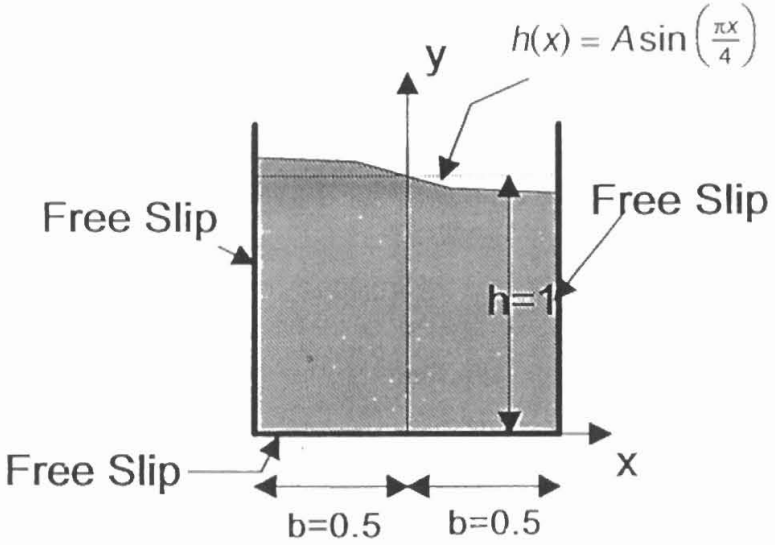

FIGURE 4 Free oscillation in a two-dimensional container with/without viscous effect.

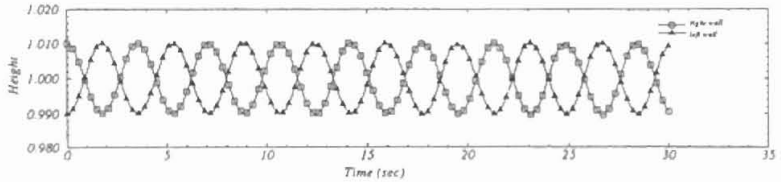

FIGURE 5 Time history of computed wave heights.

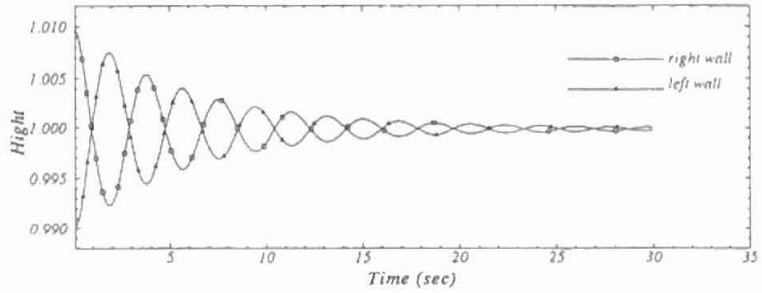

FIGURE 6 Time history of computed wave heights

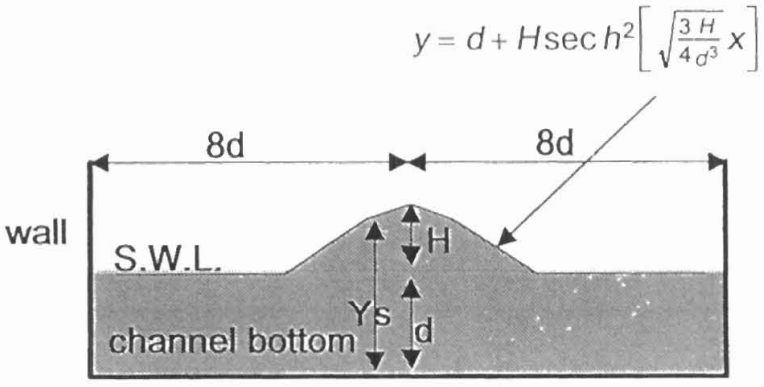

FIGURE 7 Problem definition for a solitary wave propagation.

where $g(=9.81)$ is the gravitational acceleration. For the case with $\Delta t = 0.005$ and $\Delta x = 1.333$, $\Delta y = 0.6667$, the time-varying wave heights plotted in Figure 8, show good periodicity. The water heights are well maintained and are little deteriorated by numerical damping. For comparison purposes, the run-up height R_t underlying Laitone's approximation [15].

$$R_t = 2H + \frac{d}{2}\left(\frac{H}{d}\right)^2 \tag{5.4}$$

is also plotted together with the computed results shown in Figure 8. Good agreement between two sets of solutions is clearly shown.

5.3. Liquid Sloshing in LNG Tanks

The sloshing phenomenon [16, 17] is a key to determining the limitations on tank size in a liquid cargo carrier. This subject has been the focal attention of the classification societies and the concerned regulatory bodies. Extensive studies

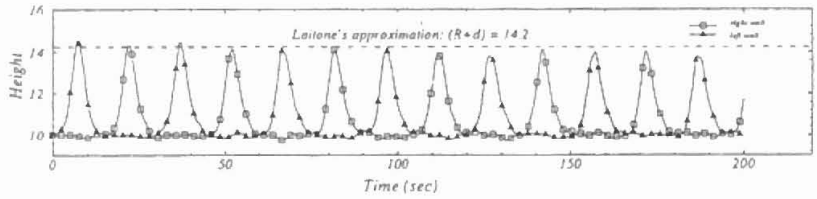

FIGURE 8 Time history of computed wave heights.

have been conducted by ship architects since 1960, when larger-sized ships became a world trend.

Figure 9 shows a rectangular tank of width 46.3 m and of depth 26 m. This tank was excited by a force given by $(g_x, g_y) = (0.01g \sin wt, -g)$, where $g = 9.81\ \text{m/sec}^2$. The response of the liquid to the tank motion of interest, among other parameters, depends also on the density, the viscosity, and the filling level of the liquid. In the present study, we considered a fairly viscous oil, leading to a Reynolds number $Re = 4743 \sim 5045$. The value of Re was computed based on the velocity Rw and the depth of undisturbed oil, R. Two heights of filling liquid, $R = 14.5$ m and 19.33 m, were considered. Different perforated baffle plates, located in the middle of the tank, were also included inthe present study.

The time-varying wave heights against the filling level, rolling frequency, length and porosity of the baffle plate, have been investigated. The evolutions of water heights with flow conditions under investigation are plotted in Figures 10–11. We have also plotted in Figures 12–13 the velocity vector fields to give insights into the general flow structure. These enlighten the role a perforated baffle plate plays in the sloshing dynamics.

As seen from Figures 14(a, b) which plot wave heights at the left wall, the baffle plate definitely has an impact on the oscillatory free surfaces. This impact is particularly prominent in cases when the rowing frequency corresponds to the resonant frequency, no matter what investigated filling levels are considered. Evident from these plots is that the flow structure changes dramatically from what without a baffle plate, implying the importance of baffle plate. From these results, we were led to conclude that the higher the baffle plate is, the smoother the water surface will be.

In situations when the oscillation frequency departs from the tank's natural frequency, the maximum wave height illustrated in Figure 14(a, b) increases slightly as the length of the

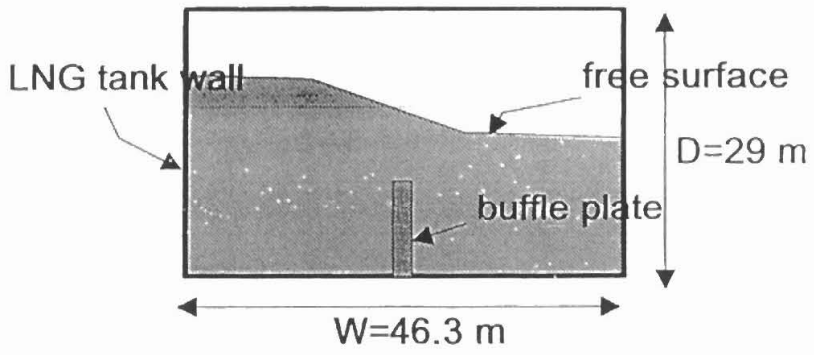

FIGURE 9 Configuration for a large amplitude sloshing problem.

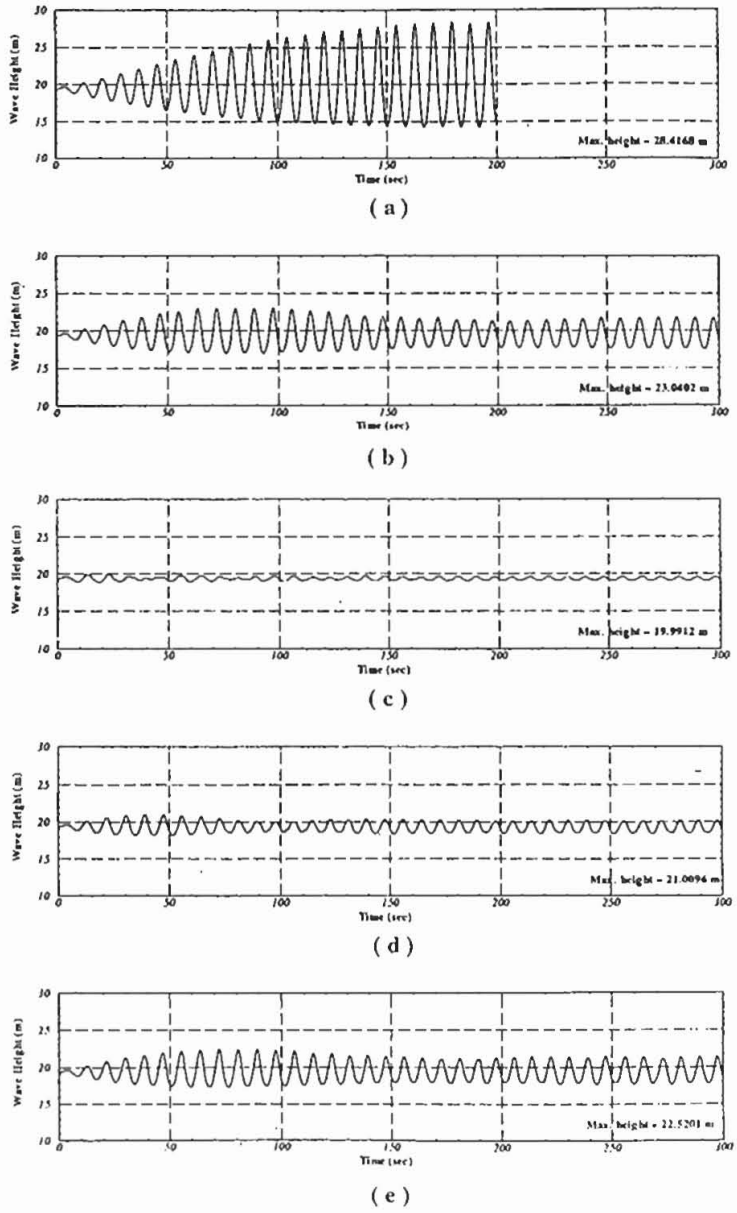

FIGURE 10 Time history of the wave height at the left wall (resonance frequency = 0.12 sec^{-1} and water level = 19.33 m) for different precentages of perforation. Dh, and lengths of baffle plate, Lb, (a) Lb = 0.0 m, (b) Lb = 7.25 m, (c) Lb = 14.5 m, (d) Lb = 14.5 m and Dh = 20%, and (e) Lb = 14.5 m and Dh = 40%.

baffle plate increases for each investigated filling level. In light of the flow structures illustrated in Figures 12 and 13, the influence of the baffle plate is clearly identified. The entire flow pattern inside the tank has been altered from that at the initial state and resembles the oscillation flow pattern in a tank which takes a half width of the original tank.

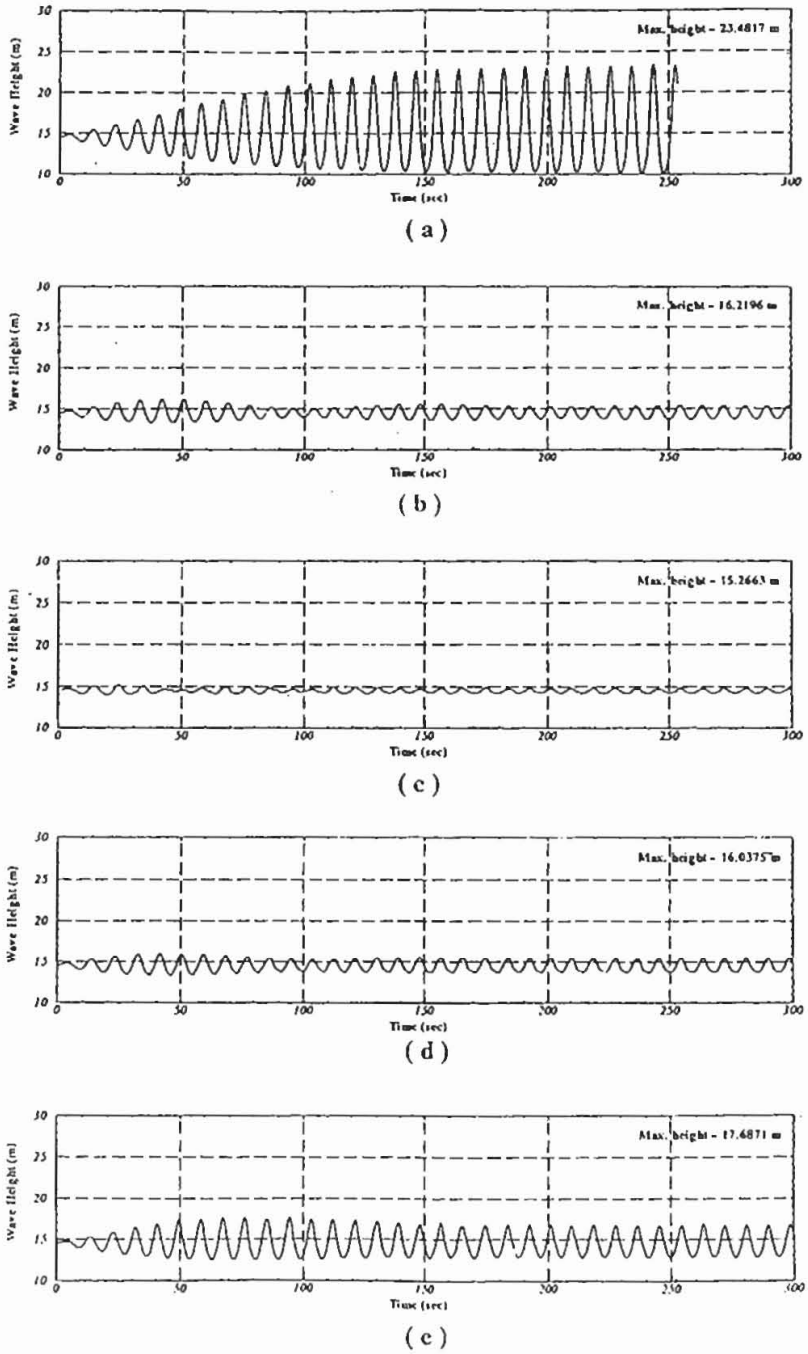

FIGURE 11 Time history of the wave height at the left wall (resonance frequency = 0.1128 sec^{-1} and water level = 14.5 m) for different percentages of perforation, Dh, and lengths of baffle plate, Lb, (a) Lb = 0.0 m, (b) Lb = 7.25 m, (c) Lb = 9.67 m, (d) Lb = 9.67 m and Dh = 20% and Dh = 40%.

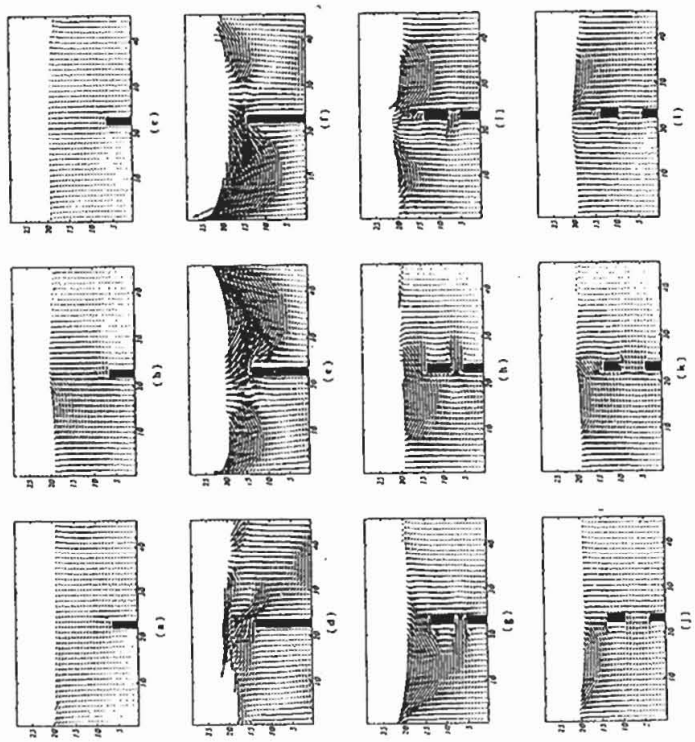

FIGURE 12 Instantaneous computed velocity fields of the liquid sloshing in an LNG tank (frequency = 0.09 sec^{-1} and water level = 19.33 m) for different lengths of baffle plate, Lb, percentage of perforation, Dh, and time, t. For (a) t = 200 sec, (b) t = 230 sec, (c) t = 260 sec, with Lb = 14.5 m at (d) t = 200 sec, (e) t = 230 sec, (f) t = 260 sec, with Lb = 14.5 m, Dh = 20% at (g) t = 200 sec, (h) t = 230 sec, (i) t = 260 sec, and with Lb = 14.5 m, Dh = 40% at (j) t = 200 sec, (k) t = 230 sec, (l) t = 260 sec.

The role that a perforated baffle plate plays is clearly demonstrated by the computed plots shown in Figures 14(c, d). At the left wall, the maximum water height for each investigated filling level is mildly increased as the baffle plate is more perforated for a tank rolling at a natural frequency. The flow structure tends to change back to that without any internal obstacle. The main reason for this variation is attributed to the fact that more fluid particles allowed to flow through the holes of the baffle plate. In contrast, the liquid heights at the left wall, as shown in Figures 12 and 13 decrease with the increase of value of porosity when the tank rolls at a frequency of 0.09 sec^{-1}. Under these circumstances, the flow structure takes a form similar to that without the baffle plate.

6. CONCLUSIONS

This paper concerns with incompressible Navier-Stokes equations in a domain bounded by a time-varying free surface. To circumvent difficulties associated with oscillatory velocities, we proposed a high-order upwinding scheme for the nonlinear convective fluxes. To tackle the problem in association with nonlinear boundary conditions at deformable surface, we have applied a donor–acceptor technique to keep track of the time-varying free surface. Two benchmark problems were used to validate the applicability of the computer program to sloshing problems. The main conclusions that can be drawn from the investigated sloshing problem are as follows:

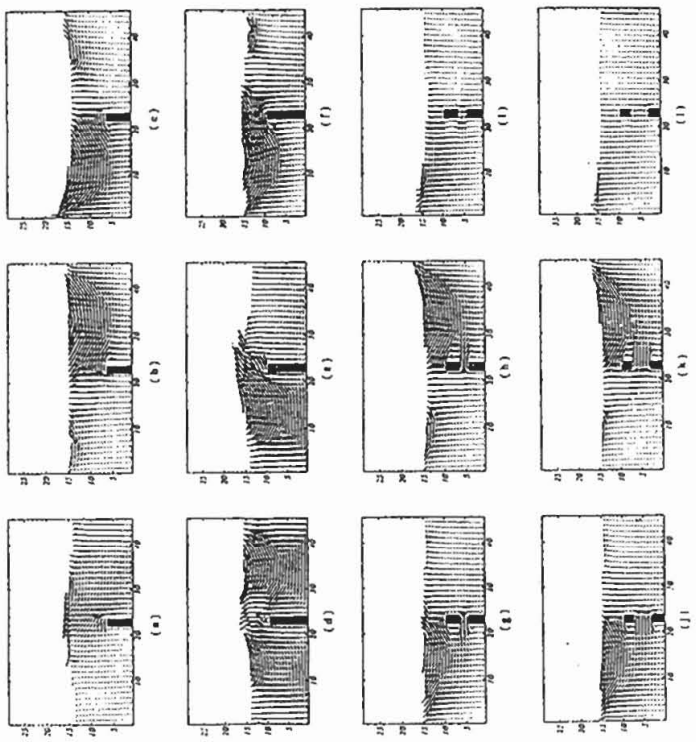

FIGURE 13 Instantaneous computed velocity fields of the liquid sloshing in an LNG tank (frequency = 0.09 sec^{-1} and water level = 14.5 m) for different lengths of baffle plate, Lb, percentages of perforation, Dh, and time, t. For (a) t = 200 sec, (b) t = 230 sec, (c) t = 260 sec, with Lb = 9.67 m at (d) t = 200 sec, (e) t = 230 sec, (f) t = 260 sec, with Lb = 9.67 m, Dh = 20% at (g) t = 200 sec, (h) t = 230 sec, (i) t = 260 sec, and with Lb = 9.67 m, Dh = 40% at (j) t = 200 sec, (k) t = 230 sec, (l) t = 260 sec.

1. There is clear evidence that at different oscillating frequencies and filling levels the internal baffle plate with/without perforated holes has great influence on the flow structure in the rolling tank. A longer baffle plate of zero porosity can mitigate the distortion of the liquid surface for a tank rolling at the resonant frequency. For the other oscillation frequencies, much distorted free surface is observed.
2. In the presence of a perforated baffle plate, the liquid oil inside the tank may flow over the baffle plate as well as flow through the drilled holes. On increase of liquid commutation, the wave heights are lowered and the degree of sloshing is lessened in conditions other than the resonant frequency. The maximum liquid height at the vertical side wall increases slightly at the resonant frequency, as compared with that for a tank having the baffle plate of length 19.33 m which is largely perforated. This statement holds regardless of the filling liquid level. In contrast to the rigid body motion at the natural frequency, the maximum heights are reduced when a larger perforated hole is encountered. A complex yet small-scale flow structure is the result.

Acknowledgements

The authors would like to express their thanks to Professor Lee Ya-Jung and Mr. Wu Chau Cheng at the USDDC for providing very useful suggestions in the course of this study. Financial support

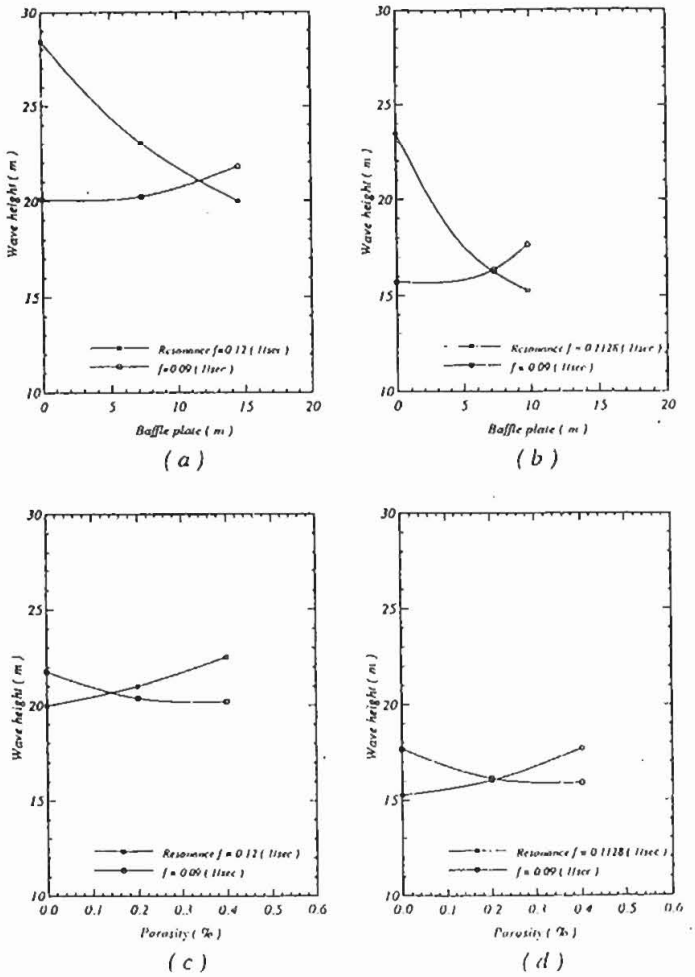

FIGURE 14 Maximum wave height at the left wall for different percentages of perforation, Dh, lengths of baffle plate, Lb, and water level, LW, (a) Dh = 0.0% and LW = 19.33 m, (b) Dh = 0.0% and LW = 14.5 m, (c) Lb = 14.5 m and LW = 19.33 m, and (d) Lb = 9.67 m and LW = 14.5 m.

from the USDDC is also acknowledged for conducting this study.

References

[1] Vreugdenhil, C. B. (1989). *Computational Hydraulics, An Introduction*, Springer-Verlag.
[2] Mei, C. C. (1989). The Applied Dynamics of Ocean Surface Waves, Advanced Series on Ocean Engineering, **1**, World Scientific.
[3] Yeung, R. W. (1982). Numerical Methods in Free-surface Flows, *Ann Rev. Fluid Mech.*, **14**, 395–422.
[4] Harlow, F. H. and Welch, J. E. (1965). Numerical Calculation of Time-dependent Viscous Incompressible Flow of Fluid with Free Surface, *Phys. Fluids*, **8**, 2102–2109.
[5] Welch, J. E., Harlow, F. H., Shannon, J. P. and Daly, B. J. (1966). A Computing Technique for Solving Viscous, Incompressible, Transient Fluid Flow Problems Involving Free Surface, LA-3425, Los Alamos Scientific Laboratory Report.
[6] Amsden, A. A. and Harlow, F. H. (1970). A Simplified MAC Technique for Incompressible Fluid Flow Calculations, *J. Comput. Phys.*, **6**, 322–325.
[7] Chan, R. K.-C. and Street, R. L. (1970). A Computer Study of Finite-amplitude Water Waves, *J. Comput. Phys.*, **6**, 68–94.
[8] Nichols, B. D. and Hirt, C. W. (1973). Calculating Three-dimensional Free Surface Flow in the Vicinity of Submerged and Exposed Structure, *J. Comput. Phys.*, **12**, 234–246.
[9] Hirt, C. W. and Nichols, B. D. (1980). Adding Limited Compressibility to Incompressible Hydrocodes, *J. Comput. Phys.*, **34**, 390–400.

[10] Hirt, C. W. and Nichols, B. D. (1981). Volume of Fluid (VOF) Method for the Dynamics of Free Boundaries, *J. Comput. Phys.*, **39**, 201–225.
[11] Nichols, B. D., Hirt, C. W. and Hotchkiss, R. S. (1980). SOLA-VOF: A Solution Algorithm for Transient Fluid Flow with Multiple Free Boundaries, LA-8355, Los Alamos Scientific Laboratory Report.
[12] Chan, R. K. C. (1975). A Generalized Arbitrary Lagrangian-Eulerian Method for Incompressible Flows with Sharp Interfaces, *J. Comput. Phys.*, **17**, 311–331.
[13] Tony, W. H. Sheu and Shi-Min Lee (1996). A Segregated Solution Algorithm for Incompressible Flows in General Coordinates, *Int. J. for Numer. Methods in Fluids*, **22**, 1–34.
[14] Ramaswamy, B., Kawahara, M. and Nakayama, T. (1986). Lagrangian Finite Element Method for the Analysis of Two-dimensional Sloshing Problems, *Int. J. for Numer. Methods in Fluids*, **6**, 659–670.
[15] Ramaswamy, B. (1990). Numerical Simulation of Unsteady Viscous Free Surface Flow, *J. Comput. Phys.*, **90**, 396–430.
[16] Huerta, A. and Liu, W. K. (1988). Viscous Flow with Large Free Surface Motion, *Computer Methods in Applied Mechanics and Engineering*, **69**, 277–324.
[17] Soulaimani, A., Fortin, M., Dhatt, G. and Ouellet, Y. (1991). Finite Element Simulation of Two- and Three-dimensional Free Surface Flows, *Computer Methods in Applied Mechanics and Engineering*, **86**, 265–296.